


Model for tectonic tremors: Enduring events, moment rate spectrum, and moment-duration scalingKota Fukuda^{*}*Earthquake Research Institute, University of Tokyo, 1-1-1 Yayoi, Bunkyo, Tokyo 113-0032, Japan*Takahiro Hatano[†]*Department of Earth and Space Science, Osaka University, 1-1 Machikaneyama, Toyonaka, Osaka 560-0043, Japan*Kimihiro Mochizuki[‡]*Earthquake Research Institute, University of Tokyo, 1-1-1 Yayoi, Bunkyo, Tokyo 113-0032, Japan* (Received 26 January 2021; revised 25 October 2021; accepted 30 November 2021; published 24 January 2022)

Numerous attempts have been made to obtain earthquake statistics from a theoretical-physics perspective, but these studies mostly involve regular earthquakes. In recent years, a new category of earthquakes, referred to as slow earthquakes, has been discovered. Slow earthquakes emit only weak or no seismic signals and have different statistics than regular earthquakes. Here we propose a physical model for the tremor, which is a type of slow earthquake, introducing two competing timescales in a cellular automaton model. The proposed model reproduces some observation results for tremors, such as enduring events, moment-duration scaling, size distribution, and the power spectrum of the moment rate function.

DOI: [10.1103/PhysRevE.105.014124](https://doi.org/10.1103/PhysRevE.105.014124)**I. INTRODUCTION****A. Statistics of regular earthquakes**

The statistical properties of nonequilibrium systems often involve power laws and have been a major research interest in statistical physics [1,2]. A prominent example is earthquakes [3], which exhibit complex time series with nontrivial statistics, including the Gutenberg-Richter (GR) law [4]. The GR law is usually stated in terms of magnitude, but the power-law nature becomes clearer if the law is recast in terms of seismic moment, which is defined as $M_0 \equiv \mu DLW$. Here μ is the shear modulus, L and W are the length and width of the fault plane where a earthquake occurs, and D is the averaged relative displacement on the fault. The probability density function of the seismic moment $P(M_0)$ can then be expressed as

$$P(M_0) \propto M_0^{-B}. \quad (1)$$

The exponent B may vary in space and time, but is generally around 1–2. Seismic activity involves yet another major power law, which is known as the Omori law [5,6], where the after-shock rate decays as a power law as the time elapses from a mainshock. In addition, the interevent time distribution, also referred to as the waiting time distribution, follows the Γ distribution [7,8]. Note that all of these nontrivial statistics are for “regular” earthquakes, whereas we consider a new category of earthquakes, i.e., slow earthquakes.

B. Low-frequency earthquakes, tectonic tremors, and slow slip events

In recent years, a new category of earthquakes has been discovered in many subduction zones in the world. This category is now referred to as slow earthquakes. They occur in the proximity of seismogenic zones, where huge earthquakes occur, and therefore the physical mechanism of slow earthquakes is of great interest as it may give a clue to the occurrence of huge earthquakes [9]. Slow earthquakes occur where the S -wave velocity is low, suggesting that fluid is involved in their occurrence mechanism [10].

One of the remarkable properties of slow earthquakes is weak seismic signals of lower frequency. Tectonic tremor is an example of slow earthquakes, showing weak seismic signals that last for several minutes to several hours [11]. Similarly, low-frequency earthquakes (LFEs) emit a weak seismic signal that lasts less than 1 s [12]. Both tremors and LFEs are slow earthquakes with a predominantly low frequency of 2–8 Hz and the seismic waveform of tremors is highly correlated with the LFE waveform. Therefore, tremors are now considered to be clusters of LFEs [13]. In particular, many observation studies have revealed that tremors are mostly the migration of many LFEs at a velocity of 10^1 – 10^2 m/s [14–16].

Tremors occur almost simultaneously with yet another type of slow earthquake [17,18], which is referred to as a slow slip event (SSE). Slow slip events do not produce any seismic waves and thus are detectable by geodetic observations only [19]. The typical slip velocity of the SSE is only several times larger than that of the steady plate motion. Slow slip events continue for longer duration, ranging from months to years.

C. Properties of tectonic tremors

Tremors have different dynamic characteristics from regular earthquakes. For regular earthquakes, the spectrum of the

^{*}k0ta2f@eri.u-tokyo.ac.jp[†]hatano@ess.sci.osaka-u.ac.jp[‡]kimi@eri.u-tokyo.ac.jp

seismic moment rate $\dot{M}_0(t)$ is proportional to f^{-2} , where f is the frequency [20]. Contrastingly, for tremors and LFEs, the spectra are proportional to f^{-1} [13,21]. Note that, in terms of the power spectrum that we discuss in this paper, they are proportional to f^{-4} and f^{-2} , respectively.

Regular and slow earthquakes obey different scaling relations. Regular earthquakes obey a distinct scaling relation with respect to their duration T and seismic moment M_0 : $T \propto M_0^{1/3}$. In contrast, slow earthquakes (tremors, LFEs, and SSEs) are known to obey another scaling: $T \propto M_0$ [21]. However, on a smaller spatiotemporal scale, this scaling may shift to $T \propto M_0^{2/3}$ [22] or $T \propto M_0^{1/3}$ [23]. This is still an open problem.

The differences in the scaling relation and the moment rate spectrum suggest that the rupture propagation dynamics of slow earthquakes are qualitatively different from those of regular earthquakes.

The statistical properties of slow earthquakes are yet to be established firmly. In particular, it is still arguable as to whether the size distribution of tremors is a power law [24–29]. For example, tremors at deeper subduction zones exhibit an exponential size distribution in terms of the radiated seismic energy [27], whereas that of the shallow tremors obeys a power-law size distribution with an exponential cutoff [28,29]. This difference may be due to the different detection limit in the seismic observation. If small events cannot be detected correctly, then the distribution function is distorted, leading to the difference in exponential or power-law distributions.

D. Models for tremors

In order to understand the underlying physics behind slow earthquakes, several models have been proposed to reproduce the spectral properties and the scaling law. For example, a pulselike fracture model was proposed to reproduce the spectral properties of tremors [30,31]. Similarly, Ide suggested that the source size of a tremor fluctuates, which is described by a stochastic differential equation for Brownian motion [32]. However, these models assumed the size of source area and therefore could not explain the size distribution.

If one wishes to clarify how the size distribution is determined within the system, one must consider rupture dynamics in spatially extended systems. In this regard, some models reproduce power-law size distributions with an exponential cutoff [33–35]. On the other hand, it is an open question as to why the size distribution of the tremor varies in different regions.

E. Olami-Feder-Christensen model

The statistical properties of regular earthquakes have been discussed using various cellular-automaton models. Among them, the Olami-Feder-Christensen (OFC) model is one of the most popular models [36–39]. The OFC model reproduces the GR law with a range of exponents for the size-frequency relation. Despite its simplicity, the model also reproduces aftershocks obeying the Omori law as well as foreshocks obeying the inverse Omori law [40,41]. These complex behaviors arising out of a simple model may be due to the complex stress heterogeneity in the model [42], which even reproduces the behavior similar to repeating earthquakes [43].

II. IMPORTANCE OF LOADING RATE

In the present study, we focus on the effect of two competing timescales in the occurrence mechanism of tremors. In regular earthquakes, the timescale of rupture propagation is sufficiently shorter than that of tectonic stress accumulation. Therefore, the loading timescale is always neglected in conventional earthquake models. Namely, stress does not accumulate during the rupture propagation [36,44,45].

For slow earthquakes, however, these two timescales may not be separated sufficiently. In order to quantify the extent of timescale separation, we define a nondimensional parameter R as

$$R \equiv \frac{\dot{\tau}}{\dot{\sigma}}, \quad (2)$$

where $\dot{\tau}$ is the stress loading rate and $\dot{\sigma}$ is the stress release rate by the slip. Therefore, we refer to R as the dimensionless loading rate. Since stress is released by the slip on the fault plane, the dimensionless loading rate represents how close the two timescales are: rupture propagation and stress accumulation.

If a patch on the fault plane is displaced by u with the rest of the area stuck, the stress change on this patch is on the order of $\mu u/L$, where L^2 is the area of the patch [46]. This also applies to the stressing case, in which a patch is stuck and the rest of the fault plane is displaced by u . Therefore, the loading rate $\dot{\tau}$ depends on the patch size L as

$$\dot{\tau} \sim \frac{\mu \dot{u}}{L}, \quad (3)$$

where \dot{u} is the steady subduction rate in the aseismic region.

In the same manner, the tectonic loading rate of a subduction zone can be estimated as $\mu \dot{u}/L$, where L is the length of a seismogenic zone. If we assume that $\dot{u} \simeq 10$ cm/yr and L is on the order of 10^2 km, then the tectonic loading rate may be on the order of 10 kPa/yr [47]. Considering that the stress drop of an earthquake is on the order of 10^{-1} – 10^0 MPa, this loading rate implies that major earthquakes (e.g., magnitude 8) that cover a seismogenic zone may occur every several 100 years. This does not contradict the seismic activities observed in major subduction zones. Then the dimensionless loading rate for regular earthquakes is roughly estimated as

$$R_{\text{RE}} \sim \frac{10 \text{ (kPa/yr)}}{10 \text{ (MPa/10 s)}} \sim 3 \times 10^{-10}, \quad (4)$$

where a stress drop of 10 MPa during a rise time of 10 s is assumed.

For tremors and LFEs, the dimensionless loading rate is estimated in the same manner. Note, however, that the major stressing source for tremors may not be a secular tectonic motion. Here we assume that tremors are driven by SSEs, since tremors and SSEs often occur simultaneously [17,19]. In this case, we regard the source region of tremors as a stuck patch and the rest area is displaced by an SSE. The stressing rate for tremors, denoted by $\dot{\tau}_{\text{TR}}$, is then estimated using Eq. (3),

$$\dot{\tau}_{\text{TR}} = \mu \frac{\dot{u}_{\text{SSE}}}{L_{\text{TR}}}, \quad (5)$$

where \dot{u}_{SSE} is the slip rate of the SSE and L_{TR} is the source region of tremors. Similarly, the stress release rate for the SSE is estimated as

$$\dot{\sigma}_{\text{SSE}} = \mu \frac{\dot{u}_{\text{SSE}}}{L_{\text{SSE}}}. \quad (6)$$

Combining Eqs. (5) and (6), we obtain the dimensionless loading rate for tremors:

$$R_{\text{TR}} = \frac{\dot{\tau}_{\text{TR}}}{\dot{\sigma}_{\text{TR}}} = \frac{L_{\text{SSE}} \dot{\sigma}_{\text{SSE}}}{L_{\text{TR}} \dot{\sigma}_{\text{TR}}}. \quad (7)$$

The source size of tremors, L_{TR} , is assumed to be 10 km because the observed locations of LFEs are clustered in this area [10]. The size of the SSE region, L_{SSE} , may be approximately 100 km. The stress release rate of SSEs, $\dot{\sigma}_{\text{SSE}}$, may be on the order of 10^{-5} – 10^{-4} kPa/s based on some observation studies. The stress drop is 10–100 kPa and the duration is 10^6 s [48,49]. The stress release rate of tremors, $\dot{\sigma}_{\text{TR}}$, may be 10 kPa/s, assuming a stress drop of 1 kPa [50] and a rise time of 0.1 s. Inserting the above values into Eq. (7), we estimate that

$$R_{\text{TR}} \sim 10^{-4}$$
– $10^{-5}. \quad (8)$

The dimensionless loading rate for tremors is still small, but much larger than that of regular earthquakes [Eq. (4)]. This is mainly because the event duration is much longer and the stress drop is much smaller for the tremors. Here we wish to investigate whether this small but finite loading rate may have some relevant effects on slip dynamics and the statistical properties of tremors.

III. MODEL DESCRIPTION

A. Algorithm

In the present study, we use the Olami-Feder-Christensen model [36,38] modified to include the stressing effect during an event. This enables us to study the competition between two timescales: rupture and loading. Such a model, however, is not new in the literature. The sandpile model [51], the forest-fire model [52], and the fiber bundle model [53] also allow such a variation, in which the cells are loaded during a toppling event. In particular, Hamon *et al.* used the OFC model in the context of solar flares, adopting the same algorithm as the present study [54]. We reinterpret and reexamine this model in the context of slow earthquakes.

The model investigated here consists of the following algorithm.

(i) *Setup.* The internal variable, ranging from 0 to h , is defined on each cell of a two-dimensional lattice of N cells. The physical meaning of the internal variable is arbitrary, while a typical interpretation is the stress.

(ii) *Inspection.* Scan all the cells. Any cells in which the internal variable exceeds the threshold h undergo slip and the internal variable drops to zero. In addition, every slipped site should redistribute the internal variable to each of the four nearest neighbors with the amount of $h\alpha$, where $0 < \alpha \leq 0.25$ and h is the stress drop. Note, however, that the redistribution process is not performed during the scan, but is just recorded to be implemented in the next step. Thus, each cell needs to be inspected only once at each time step.

(iii) *Update.* After scanning all of the sites, the redistribution process is performed. At the same time, each cell is loaded with $\dot{\tau} \Delta t$. The moment rate $\dot{M}_o(t)$ is defined as the number of slipped sites.

After process (iii), go back to process (ii) with the time elapsed $t \rightarrow t + \Delta t$.

With this algorithm, an event takes a finite time and therefore the duration is defined. A single event continues as long as the moment rate is nonzero: $\dot{M}_o(t) > 0$ for $t_i \leq t \leq t_f$. Namely, the event starts when $\dot{M}_o(t_i) > 0$ with $\dot{M}_o(t_i - \Delta t) = 0$ and terminates when $\dot{M}_o(t_f + \Delta t) = 0$. The total moment release of an event is then defined as

$$M_o = \int_{t_i}^{t_f} \dot{M}_o(t) dt \quad (9)$$

and the duration of this event is $t_f - t_i$.

A stress drop of h occurs during a single time step Δt and therefore the stress release rate is given by $\dot{\sigma} = h/\Delta t$. The dimensionless loading rate is thus written as $R = \dot{\tau} \Delta t/h$. In the numerical simulation, Δt and h are set to unity and therefore the stress increase at each time step $\dot{\tau} \Delta t$ is R . By varying the dimensionless loading rate R , we can investigate the effect of stress accumulation during rupture propagation.

The difference between the present model and the conventional OFC model is the stressing effects during an event. In this model, each cell is stressed even during an event. This is implemented in step (iii). In the conventional OFC model, cells are not stressed during a sequence of toppling events. In this respect, the present model is reduced to the conventional model in the limit of $R \rightarrow 0$.

Note that the moment rate $\dot{M}_o(t)$ is obtained as time series data. Theoretically, the moment rate is proportional to the absolute value of the displacement waveform in the far-field observation. Therefore, the simulation results of this model can be discussed in relation to the observed waveforms. Such a quantity is absent in the conventional OFC model. In this sense, we may refer to the present model as a dynamic OFC model.

We adopt open boundary conditions, where the internal variable is discarded at the boundary upon redistribution.

Note that this model does not allow the fast numerical algorithm proposed by Pinho and Prado [55]. The computational cost is thus proportional to the square of the number of cells. For this reason, we cannot deal with a very large system in this study.

B. Physical interpretation

Here the entire system is assumed to be a source region of tremors, the size of which is known to be on the order of several kilometers [21,56]. We consider a single source region only and exclude multiple source regions and their interactions.

Physically, the slip and stress redistributions in steps (ii) and (iii), constituting a single time step of the model, take a certain amount of time Δt . For tremors, this duration for stress redistribution should be much longer than that for regular earthquakes and therefore the amount of stress accumulation during Δt may not be negligible. This slow redistribution of stress may be because stress redistribution is not caused by

the elasticity alone but may rather be due to fluid migration or any other slow processes at the plate boundaries. Then the nearest-neighbor interaction adopted here may model such fluid-induced stress redistribution and may not be a mere oversimplification.

The slip propagates over the cell size of Δx during a single time step. Thus, Δt is determined by Δx and the slip propagation velocity.

In cellular automata, one cannot take the limit of $\Delta x \rightarrow 0$ since it is the only length scale in the system. Accordingly, the OFC model and the Burridge-Knopoff model [44,45] are essentially discrete models in the sense that they do not have the continuum limit [57]. This spatial discreteness in cellular automata has been criticized in earthquake studies. However, in considering geological heterogeneities in natural faults, it is not so obvious as to whether they can be modeled as a continuum. They may have some characteristic wavelengths, which would validate discrete modeling [58,59]. In other words, the cells in this model may represent a characteristic spatial heterogeneity in the plate boundaries, i.e., the roughness, or inhomogeneities of permeability and rheological properties.

IV. RESULTS

A. Steady state

In the conventional OFC model, the statistical distribution is discussed in the steady state after a sufficient time step. We evaluate and analyze the steady state in the dynamic OFC model based on the behavior of the moment rate power spectrum. Figure 1 shows the power spectrum of the moment rate after time steps of $t = 10^5, 10^6, 10^7$ from the initial state. The power spectrum is regarded as the Lorentzian expressed in the following equation:

$$I(f) = \frac{a}{1 + (f/f_c)^2}. \quad (10)$$

Since the behavior of the power spectrum is Lorentzian, we define the inverse of the corner frequency f_c as the correlation time τ . The corner frequency f_c decreases over time in Fig. 1.

Figure 2 shows the evolution of the correlation time τ with the elapsed time t . The points are the ensemble averages of ten simulation runs with different initial conditions and the error bars indicate 1σ . When the dissipation parameter is small or R is small, the number of events in the time series for determining the power spectrum is reduced and thus the fluctuations become larger. The correlation time increases with time and then becomes constant after a certain transient time. This is interpreted as a steady state. Figure 2 shows that the relaxation time decreases as R or the dissipative parameter increase. Note that the correlation time at a steady state does not depend on the dimensionless loading rate and the dissipative parameter.

Figure 3 shows the correlation times for various system sizes with $R = 1 \times 10^{-5}$. The steady-state correlation time increases for a larger system. However, the time to reach a steady state is independent of the system size. Based on these results, we estimate the time t_{ss} to reach a steady state, as shown in Table I, and use the data from t_{ss} onward for further discussion.

Figure 4 shows how the steady-state correlation time τ_{ss} depends on the number of cells at $R = 1 \times 10^{-5}$. It is described

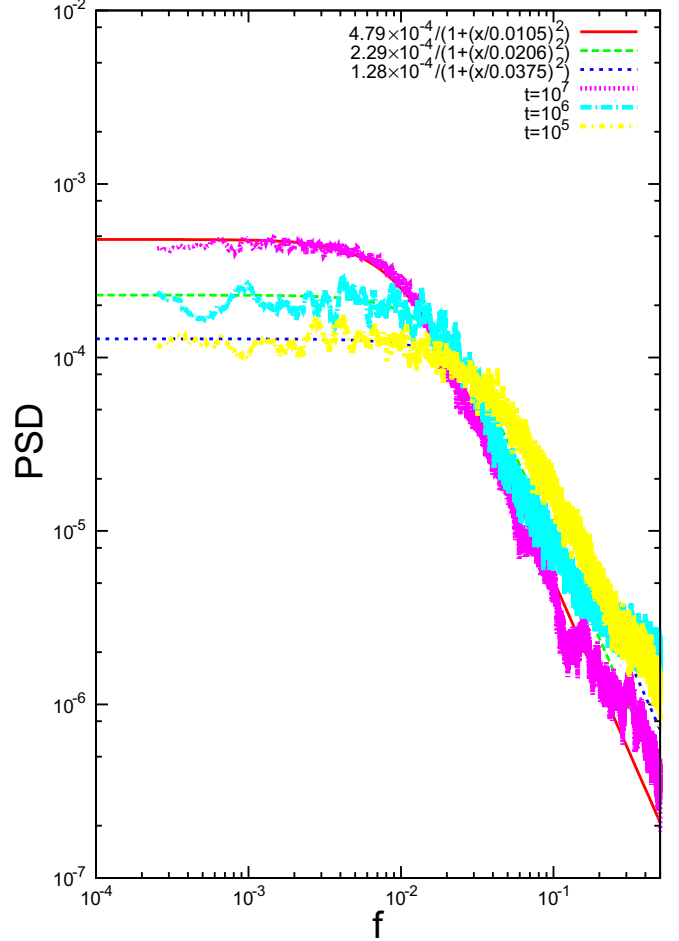


FIG. 1. Power spectrum of the moment rate after time steps $t = 10^5, 10^6, 10^7$ from the initial state. The dimensionless loading rate $R = 1 \times 10^{-6}$ with $N = 60 \times 60$ cells. This power spectrum is computed from the 2^{17} time-step data and smoothed by the moving average of 60 data points.

as $\tau_{ss} \propto N^\omega$, where the index ω takes a range of values from 0.47 to 0.61. However, since this scaling is confirmed only for 1.5 orders of magnitude, the power-law behavior may not be decisive. At least, a positive dependence exists.

In the conventional OFC model, the transition to steady states is studied by monitoring the snapshots of the stress field and the steady state is characterized by the disappearance of the characteristic structure [60]. In the present model, we also observe the snapshots of stress field and find the same tendency.

TABLE I. Approximate time t_{ss} required for the steady state.

α	$R = 10^{-6}$	$R = 10^{-5}$	$R = 10^{-4}$	$R = 5 \times 10^{-4}$
0.21	10^8	10^8	10^7	10^6
0.22	10^8	10^8	10^7	10^6
0.23	10^8	10^8	10^7	10^6
0.24	10^7	10^7	10^6	10^6

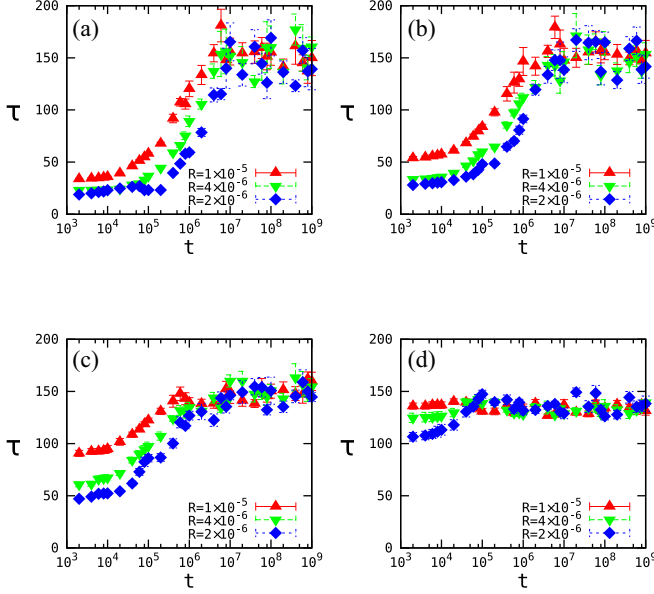


FIG. 2. Evolution of the correlation time τ with the elapsed time t for $N = 60 \times 60$ cells and (a) $\alpha = 0.21$, (b) $\alpha = 0.22$, (c) $\alpha = 0.23$, and (d) $\alpha = 0.24$. The plot points are ensemble averages of ten data with different initial conditions and the error bars indicate 1σ .

B. Enduring events and size distribution

Figure 5 shows the representative time series of the moment rate at some loading rates. We can see that the duration of an event increases as the dimensionless loading rate increases. To show this quantitatively, the average duration $\langle T \rangle$ is computed for 10^6 events at each condition. As shown in Fig. 6, the average duration increases exponentially with the dimensionless loading rate, i.e., $\langle T \rangle = A \exp(R/R_c)$. Here A

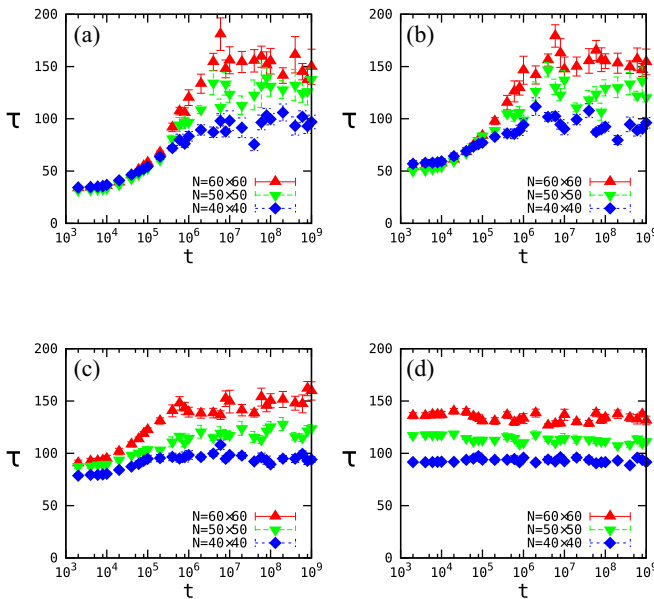


FIG. 3. Evolution of the correlation time τ with the elapsed time t for various system sizes (a) $\alpha = 0.21$, (b) $\alpha = 0.22$, (c) $\alpha = 0.23$, and (d) $\alpha = 0.24$, with $R = 1 \times 10^{-5}$.

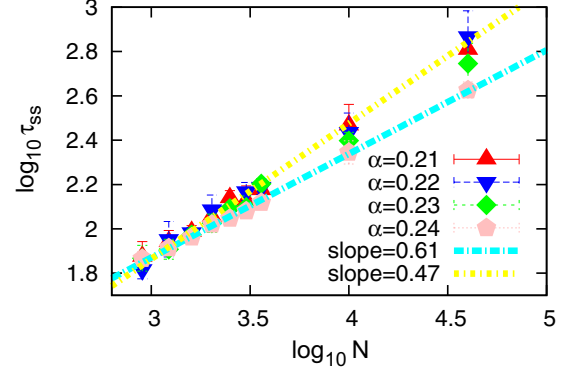


FIG. 4. Steady-state correlation time τ_{ss} dependence on system size at $R = 1 \times 10^{-5}$. The lines represent a power law of $\tau_{ss} \propto N^\omega$, where the index ω ranges from 0.47 to 0.61.

and R_c are parameters and R_c represents the characteristic dimensionless loading rate for the exponential increase.

Figure 7 shows the relationship between the characteristic dimensionless loading rate and the number of cells for each of the different dissipation parameters. The characteristic loading rate obeys a scaling $1/R_c \propto N^\gamma$ with γ depending on α .

Figure 8 shows the probability density functions for the moment and for the duration. At smaller loading rates, the distribution function for the moment may be regarded as a power law up to two orders of magnitude, whereas that for duration is not a clear power law. Both probability density functions have a peak at large R . This peak corresponds to the system-size event. However, the mechanism for this peak is not clear at this point.

In the present model, each event has a finite duration and therefore the definition of aftershocks is not apparent. We

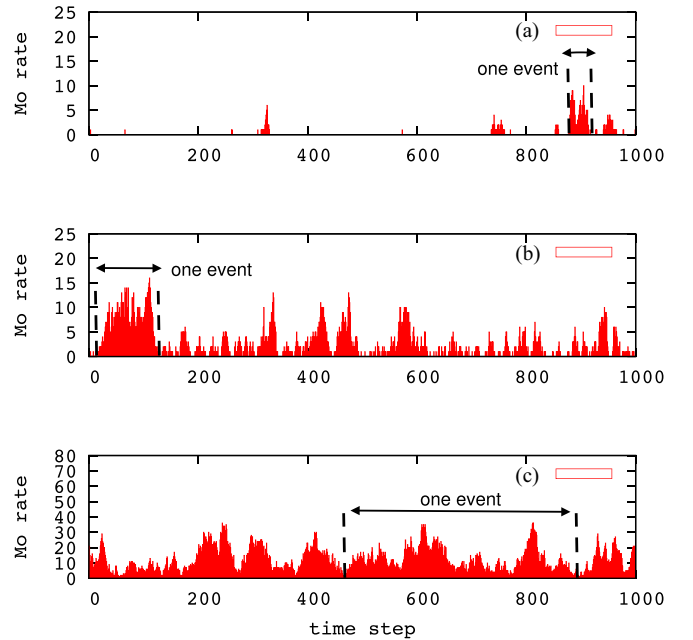


FIG. 5. Time series of the moment rate at (a) $R = 1 \times 10^{-5}$ and $R/R_c = 0.102$, (b) 1×10^{-4} and $R/R_c = 1.02$, and (c) 5×10^{-4} and $R/R_c = 5.10$ for $N = 60 \times 60$ cells and $\alpha = 0.22$.

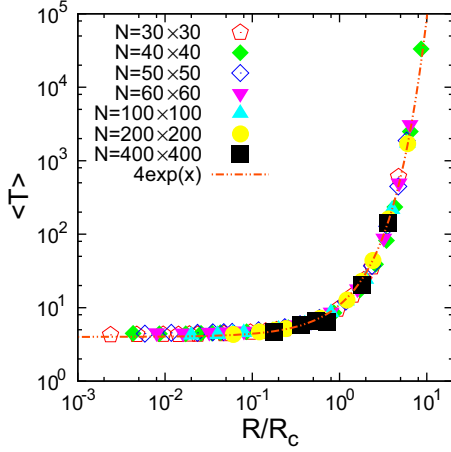


FIG. 6. Average duration of 10^6 events $\langle T \rangle$ obtained from the simulation for each dimensionless loading rate and $N = 30 \times 30$, 40×40 , 50×50 , 60×60 , 100×100 , 200×200 , and 400×400 cells, for $\alpha = 0.22$. The average duration shows an exponential increase in the dimensionless loading rate, which can be expressed as $\langle T \rangle = A \exp(R/R_c)$.

thus do not inspect the Omori law in this model. On the other hand, the waiting time distribution is well defined and found to be the Weibull distribution that is very close to the exponential distribution irrespective of the loading rate R . This behavior is consistent with the conventional OFC model [40,61]. However, this waiting time distribution does not agree with those observed for natural earthquakes [7,8]. This is a common drawback of the OFC model.

C. Dimensionless loading rate dependence of the moment rate spectrum

Figure 9 shows the power spectrum of moment rate, which may be regarded as Lorentzian for $R < R_c$. Then the lower-frequency part decreases at $R \simeq R_c$. For $R > R_c$, the shape

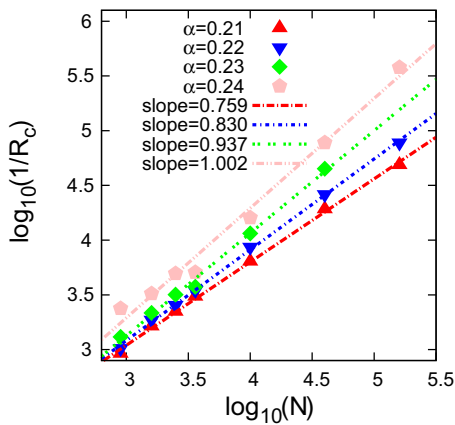


FIG. 7. Relationship between the characteristic dimensionless loading rate R_c and the number of cells for each of the dissipation parameters. The characteristic dimensionless loading rate obeys a scaling $1/R_c \propto N^\gamma$, where $\gamma = 0.759$ ($\alpha = 0.21$), $\gamma = 0.830$ ($\alpha = 0.22$), $\gamma = 0.937$ ($\alpha = 0.23$), and $\gamma = 1.002$ ($\alpha = 0.24$).

of the power spectrum develops a peak and deviates from Lorentzian.

D. Moment-duration scaling

Figure 10 shows the relationship between the event duration and the moment. The linear scaling relation $M_o \propto T$ holds for larger events ($T > \tau_{ss}$ and $M_o > N$). Such scaling may be caused by finite-size effects. For smaller events ($T < \tau_{ss}$ and $M_o < N$), another scaling relation $M_o \propto T^E$ holds. Here the exponent E depends on the dissipative parameter and ranges from 1.55 to 1.90, namely, the scaling relationship between the moment and the duration transitions around the correlation time ($T \simeq \tau_{ss}$) and the system size ($M_o \simeq N$).

At $R < R_c$, larger events do not occur and therefore the linear scaling relation does not appear. Accordingly, there is only one scaling regime for smaller events.

V. DISCUSSION

A. Pulselike rupture

The self-similar nature of regular earthquakes is expressed as $L \propto D \propto T$, where T is the duration, L is the characteristic length of the fault, and D is the average slip amount. In the proposed model, the seismic moment is defined in terms of the number of toppled cells, as the amount of slip is set to be constant. Accordingly, the present model presumes a pulselike rupture, because the slip amount D is independent of the duration. In addition, we observe that the rupture propagates unilaterally in this model. Because of the constant slip amount and the unilateral rupture propagation, the shape of the moment rate is boxcarlike, as shown in Fig. 5. This implies that the moment rate spectrum is proportional to the -1 power of the frequency. (The power spectrum is of the -2 power.) In our simulation, this behavior remains in the limit of $R \rightarrow 0$.

B. Collective nature of the tremor

In the present model, the stress loading causes more toppling sites and therefore a single event tends to endure. This tendency is enhanced for a larger loading rate or a smaller stress release rate, i.e., larger R . As a result, the event duration increases for larger R . In this sense, the present model reproduces the characteristics of tremors, which continue for a certain duration with the successive occurrence of unit events. Namely, a tremor is a swarm (collective occurrence) of LFEs, whereas an event in the present model consists of many successive toppling events.

C. Area characteristics of size-frequency relation

Despite recent extensive studies, the size-frequency relation for tremors is still not conclusive [24–28], partly due to the various detectability limits in observations. As shown in Fig. 8, the size-frequency relation suggests that the characteristic event emerges for $R > R_c$, while it is scale-free for $R < R_c$. Thus, the regional or depth dependence of R/R_c may explain various observation studies on the size-frequency distribution. However, R_c cannot be inferred for plate boundaries, whereas R can be estimated using observable quantities. In the present model, R_c depends on the number of cells N .

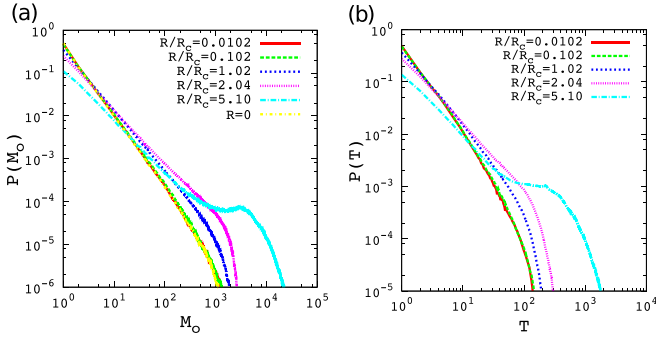


FIG. 8. Probability density functions of (a) the moment and (b) the duration. The dissipation parameter is 0.22 and $N = 60 \times 60$. The dimensionless moment rates are $R = 10^{-6}$ ($R/R_c = 0.010$), $R = 10^{-5}$ ($R/R_c = 0.102$), $R = 10^{-4}$ ($R/R_c = 1.02$), and $R = 5 \times 10^{-4}$ ($R/R_c = 5.10$). The results obtained from the conventional OFC model are shown for $R = 0$.

This is determined by the cell size Δx , which may be the characteristic wavelength of geological heterogeneity. This is not observable to date.

D. Moment-duration scaling

Figure 10 indicates that the scaling transition occurs when the seismic moment is roughly equal to the total number of cells and the event duration approximately equals the correlation time. The scaling relation $M_o \propto T$ is observed only above this transition point. Since $M_o > N$, cells slip more than once in this regime. If τ is the number of time steps needed for N cells to slip, then the duration should be $\tau M_o/N$ when $M_o > N$.

At the transition point, all of the cells undergo slip once on average, where $M_o \simeq N$ and $T \simeq \tau_{ss}$. The correlation time τ_{ss} is thus interpreted as the characteristic time for the rupture to propagate through the system.

The proposed model thus reproduces the scaling law for slow earthquakes, i.e., $M_o \propto T$ [21], but this is true only when $R/R_c > 1$. In this regime, the moment-rate power spectrum deviates from Lorentzian and develops a peak at a low frequency. Although such a peak has not been reported in observations, it may be masked by microseism, which is dominant in the frequency range from 1 mHz to 1 Hz [62]. If we can somehow unmask microseism, a direct verification of our result may be feasible. At the same time, we cannot exclude the possibility that some other kinds of slip occur on the low-frequency side. In that case, the model should be improved to include such processes.

E. Comparison with other tremor models

There have been several similar models in the literature. Among them, the model in [30] assumes many brittle patches that cause LFEs driven by SSEs in the continuum plate boundary. The implementation of brittle patches in the continuum is similar to the assumption of discrete cells that topple in the present model. In this respect, the present model may be regarded as a simplification of distributed patches in the continuum. As a result, both models can reproduce the mo-

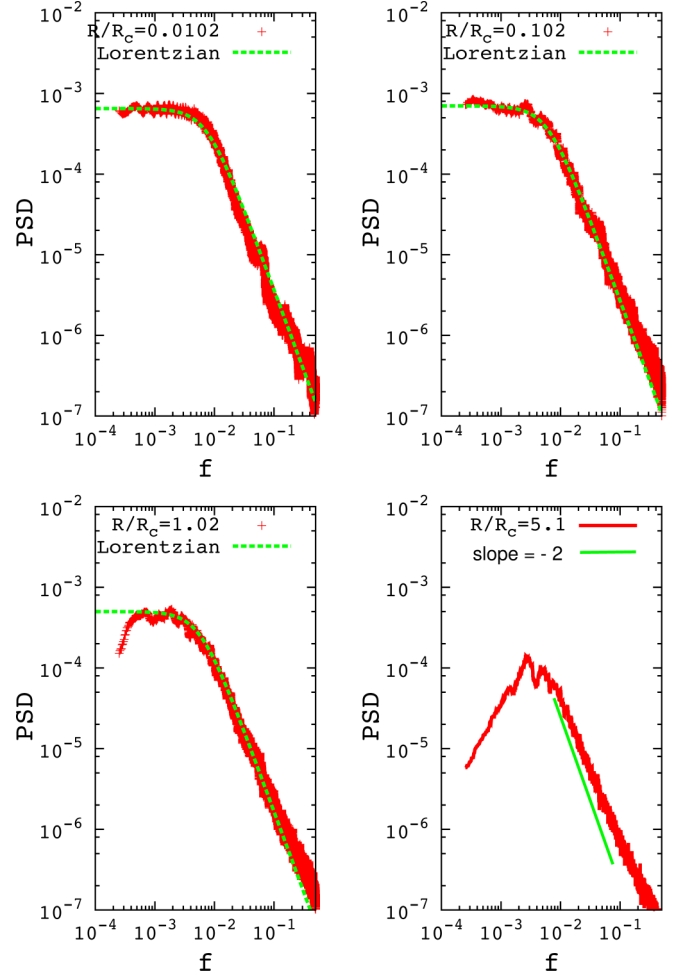


FIG. 9. Moment rate power spectrum for $N = 60 \times 60$ cells and $\alpha = 0.22$. The power spectrum is Lorentzian only for $R < R_c$, while the lower-frequency component declines at larger R .

ment rate spectrum proportional to f^{-1} . On the other hand, a major difference is the interaction between patches or cells. The elasticity yields long-range interaction between patches in the continuum, whereas the nearest-neighbor interaction is adopted in the present model. Nevertheless, they yield similar behavior. This similarity, despite the apparent difference in the models, may be an interesting problem to investigate further.

Another model [33] also assumes a collection of cellular slip patches on a fault surrounded by an elastic continuum. Adopting a depth-dependent friction model, the complex slip behavior similar to migrating tremors is reproduced and the size-frequency relation is a power law with exponential cutoff. On the other hand, the scaling relation is rather peculiar: $M_o \propto T^2/\log(T)^{2/3}$. In addition, the nature of moment rate is not discussed. Considering the complexity of the model settings, these continuum models [30,33] rather illuminate a success of the present model, which is quite simple but reproduces the moment rate behavior and the scaling relation.

Apart from continuum models, another cellular automaton model has been proposed aiming in the same direction as the present study. This model [35] adopts a stochastic nearest-neighbor interaction and reproduces the moment rate behavior

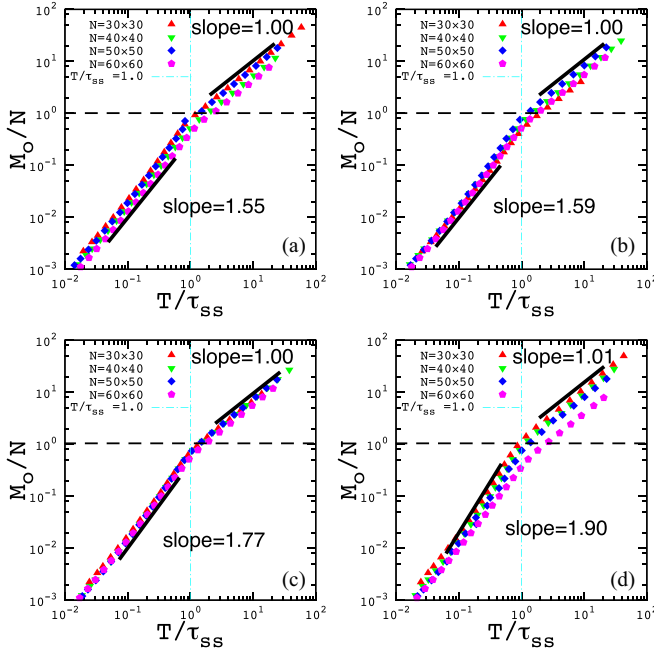


FIG. 10. Relationship between the event duration and the moment at different system sizes (a) $\alpha = 0.21$, (b) $\alpha = 0.22$, (c) $\alpha = 0.23$, and (d) $\alpha = 0.24$ and different dissipation parameters at $R/R_c > 1$. We set logarithmic bins for duration and compute the averaged moment for the events that belong to each bin. The average is taken using 10^6 events at each set of system size and dissipation parameter. The averaged moment and the duration are then rescaled by the number of cells and the correlation time, respectively. The events with a duration longer than the correlation time obeys the relationship $M_o \propto T$. Shorter duration events obey $M_o \propto T^E$, where E depends on the dissipative parameter and ranges from 1.55 to 1.90.

and the moment-duration scaling. The discrete nature is common to our model, but the algorithm is significantly different (particularly the stochastic dynamics). The physical meaning of this stochastic interaction is not clear at this point. In contrast, in the present model, the time evolution is deterministic and the randomness comes into play only in the initial state. In other words, complex dynamic behavior emerges out of the spatial heterogeneity of the stress. In this respect, the physical meaning may be clearer in the present model.

F. Criticism of nearest-neighbor interaction

The argument for ignoring far-field interactions may be useful when considering the model of tremors. Many studies have suggested that areas where tremors occur are fluid rich [10]. Therefore, we may assume that the pore fluid pressure is

essential for tremors. Based on this consideration, the stress carrier in slip propagation is mainly the dynamics of the pore fluid pressure. The nearest-neighbor interaction in the proposed model might be somewhat justified by such fluid-assisted rupture propagation.

The correlation time, which is defined through the power spectrum of the moment rate, is the time required for rupture propagation through the system. This implies that the memory in the system is not lost until all of the sites are toppled. This timescale is independent of the loading rate and thus rather intrinsic.

Generally, the state variable on the cells may undergo superdiffusion. This is apparent from Fig. 4, where the correlation time depends on the system size N with an exponent that is much larger than that for diffusion. Note, however, that this interpretation does not apply for the case of $\alpha = 0.24$, because the scaling does not completely hold, as shown in Fig. 10.

VI. CONCLUSION

We have proposed a simple model for tremors, modifying a cellular automaton model to incorporate two competing timescales: stressing and destressing rates. This ratio, denoted by R , plays a central role in reproducing the dynamical properties of tremors. By carefully removing the transient effects, we can discuss the steady-state properties properly. Some features of tremors are reproduced at rather larger loading rates, implying that the ratio of the above two rates is a key parameter for dynamics of tremors.

As opposed to most self-organized criticality models, a rupture (or an avalanche) propagates within finite time steps. We can thus define the duration of a single event and the duration-moment relation. The event duration increases exponentially with the dimensionless loading rate, leading to enduring events.

Nearest-neighbor interaction, which is often criticized from the viewpoint of elasticity, may be regarded as fluid-assisted stress diffusion. However, more critical inspection would be necessary on the relevance of the model to natural plate boundaries, particularly the counterparts of the discrete cell size, the finite time step, and the dissipation parameter.

ACKNOWLEDGMENTS

The present study was supported by the Japan Society for the Promotion of Science through Grants-in-Aid for Scientific Research (KAKENHI) No. 16H06478 and No. 19H01811. We used the computer systems of the Earthquake and Volcano Information Center of the Earthquake Research Institute, University of Tokyo.

[1] P. Bak, C. Tang, and K. Wiesenfeld, Self-Organized Criticality: An Explanation of the $1/f$ Noise, *Phys. Rev. Lett.* **59**, 381 (1987).
 [2] P. Bak, C. Tang, and K. Wiesenfeld, Self-organized criticality, *Phys. Rev. A* **38**, 364 (1988).

[3] A. Sornette and D. Sornette, Self-organized criticality and earthquakes, *Europhys. Lett.* **9**, 197 (1989).
 [4] B. Gutenberg and C. F. Richter, Frequency of earthquakes in California, *Bull. Seismol. Soc. Am.* **34**, 185 (1944).

- [5] F. Omori, On the aftershocks of earthquakes, *J. Coll. Sci. Imp. Univ. Jpn.* **7**, 111 (1894).
- [6] T. Utsu, Aftershocks and earthquake statistics (1): Some parameters which characterize an aftershock sequence and their interrelations, *J. Fac. Sci. Hokkaido Univ. Ser. 7* **3**, 129 (1970).
- [7] A. Corral, Local distributions and rate fluctuations in a unified scaling law for earthquakes, *Phys. Rev. E* **68**, 035102(R) (2003).
- [8] A. Corral, Long-Term Clustering, Scaling, and Universality in the Temporal Occurrence of Earthquakes, *Phys. Rev. Lett.* **92**, 108501 (2004).
- [9] K. Obara and A. Kato, Connecting slow earthquakes to huge earthquakes, *Science* **353**, 253 (2016).
- [10] D. R. Shelly, G. C. Beroza, S. Ide, and S. Nakamura, Low-frequency earthquakes in Shikoku, Japan, and their relationship to episodic tremor and slip, *Nature (London)* **442**, 188 (2006).
- [11] K. Obara, Nonvolcanic deep tremor associated with subduction in southwest Japan, *Science* **296**, 1679 (2002).
- [12] A. Katsumata and N. Kamaya, Low-frequency continuous tremor around the Moho discontinuity away from volcanoes in the southwest Japan, *Geophys. Res. Lett.* **30**, 20-1 (2003).
- [13] D. R. Shelly, G. C. Beroza, and S. Ide, Non-volcanic tremor and low-frequency earthquake swarms, *Nature (London)* **446**, 305 (2007).
- [14] D. R. Shelly, G. C. Beroza, and S. Ide, Complex evolution of transient slip derived from precise tremor locations in western Shikoku, Japan, *Geochem. Geophys. Geosyst.* **8**, 10 (2007).
- [15] A. Ghosh, J. E. Vidale, J. R. Sweet, K. C. Creager, A. G. Wech, H. Houston, and E. E. Brodsky, Rapid, continuous streaking of tremor in Cascadia, *Geochem. Geophys. Geosyst.* **11**, 12 (2010).
- [16] K. Obara, T. Matsuzawa, S. Tanaka, and T. Maeda, Depth-dependent mode of tremor migration beneath Kii Peninsula, Nankai subduction zone, *Geophys. Res. Lett.* **39**, 10308 (2012).
- [17] G. Rogers and H. Dragert, Episodic tremor and slip on the Cascadia subduction zone: The chatter of silent slip, *Science* **300**, 1942 (2003).
- [18] Y. Ito, K. Obara, K. Shiomi, S. Sekine, and H. Hirose, Slow earthquakes coincident with episodic tremors and slow slip events, *Science* **315**, 503 (2007).
- [19] H. Hirose, K. Hirahara, F. Kimata, N. Fujii, and S. Miyazaki, A slow thrust slip event following the two 1996 Hyuganada earthquakes beneath the Bungo Channel, southwest Japan, *Geophys. Res. Lett.* **26**, 3237 (1999).
- [20] K. Aki, Scaling law of seismic spectrum, *J. Geophys. Res.* **72**, 1217 (1967).
- [21] S. Ide, G. C. Beroza, D. R. Shelly, and T. Uchide, A scaling law for slow earthquakes, *Nature (London)* **447**, 76 (2007).
- [22] S. Ide, K. Imanishi, Y. Yoshida, G. C. Beroza, and D. R. Shelly, Bridging the gap between seismically and geodetically detected slow earthquakes, *Geophys. Res. Lett.* **35**, L10305 (2008).
- [23] J. Gomberg, A. Wech, K. Creager, K. Obara, and D. Agnew, Reconsidering earthquake scaling, *Geophys. Res. Lett.* **43**, 6243 (2016).
- [24] T. Watanabe, Y. Hiramatsu, and K. Obara, Scaling relationship between the duration and the amplitude of non-volcanic deep low-frequency tremors, *Geophys. Res. Lett.* **34**, L07305 (2007).
- [25] Y. Hiramatsu, T. Watanabe, and K. Obara, Deep low-frequency tremors as a proxy for slip monitoring at plate interface, *Geophys. Res. Lett.* **35**, L13304(2008).
- [26] H. Kao, K. Wang, H. Dragert, J. Y. Kao, and G. Rogers, Estimating seismic moment magnitude (M_w) of tremor bursts in northern Cascadia: Implications for the “seismic efficiency” of episodic tremor and slip, *Geophys. Res. Lett.* **37**, L19306 (2010).
- [27] S. Yabe and S. Ide, Spatial distribution of seismic energy rate of tectonic tremors in subduction zones, *J. Geophys. Res.: Sol. Ea.* **119**, 8171 (2014).
- [28] M. Nakano, S. Yabe, H. Sugioka, M. Shinohara, and S. Ide, Event size distribution of shallow tectonic tremor in the Nankai trough, *Geophys. Res. Lett.* **46**, 5828 (2019).
- [29] M. Nakano and S. Yabe, Changes of event size distribution during episodes of shallow tectonic tremor, Nankai trough, *Geophys. Res. Lett.* **48**, e2020GL092011 (2021).
- [30] R. Ando, R. Nakata, and T. Hori, A slip pulse model with fault heterogeneity for low-frequency earthquakes and tremor along plate interfaces, *Geophys. Res. Lett.* **37**, L10310 (2010).
- [31] R. Nakata, R. Ando, T. Hori, and S. Ide, Generation mechanism of slow earthquakes: Numerical analysis based on a dynamic model with brittle-ductile mixed fault heterogeneity, *J. Geophys. Res.: Sol. Ea.* **116**, B08308(2011).
- [32] S. Ide, A Brownian walk model for slow earthquakes, *Geophys. Res. Lett.* **35**, L17301 (2008).
- [33] Y. Ben-Zion, Episodic tremor and slip on a frictional interface with critical zero weakening in elastic solid, *Geophys. J. Int.* **189**, 1159 (2012).
- [34] D. Zigone, Y. Ben-Zion, and M. Campillo, Modelling non-volcanic tremor, slow slip events and large earthquakes in the Guerrero subduction zone (Mexico) with space-variable frictional weakening and creep, *Geophys. J. Int.* **202**, 653 (2015).
- [35] S. Ide and S. Yabe, Two-dimensional probabilistic cell automaton model for broadband slow earthquakes, *Pure Appl. Geophys.* **176**, 1021 (2019).
- [36] Z. Olami, H. J. S. Feder, and K. Christensen, Self-Organized Criticality in a Continuous, Nonconservative Cellular Automaton Modeling Earthquakes, *Phys. Rev. Lett.* **68**, 1244 (1992).
- [37] Z. Olami and K. Christensen, Temporal correlations, universality, and multifractality in a spring-block model of earthquakes, *Phys. Rev. A* **46**, R1720 (1992).
- [38] K. Christensen and Z. Olami, Scaling, phase transitions, and nonuniversality in a self-organized critical cellular-automaton model, *Phys. Rev. A* **46**, 1829 (1992).
- [39] K. Christensen and Z. Olami, Variation of the Gutenberg-Richter b values and nontrivial temporal correlations in a spring-block model for earthquakes, *J. Geophys. Res.: Sol. Ea.* **97**, 8729 (1992).
- [40] S. Hergarten and H. J. Neugebauer, Foreshocks and Aftershocks in the Olami-Feder-Christensen Model, *Phys. Rev. Lett.* **88**, 238501 (2002).
- [41] A. Helmstetter, S. Hergarten, and D. Sornette, Properties of foreshocks and aftershocks of the nonconservative self-organized critical Olami-Feder-Christensen model, *Phys. Rev. E* **70**, 046120 (2004).
- [42] S. Hergarten and R. Krenn, Synchronization and desynchronization in the Olami-Feder-Christensen earthquake model and potential implications for real seismicity, *Nonlin. Process. Geophys.* **18**, 635 (2011).
- [43] H. Kawamura, T. Yamamoto, T. Kotani, and H. Yoshino, Asperity characteristics of the Olami-Feder-Christensen model of earthquakes, *Phys. Rev. E* **81**, 031119 (2010).

- [44] R. Burridge and L. Knopoff, Model and theoretical seismicity, *Bull. Seismol. Soc. Am.* **57**, 341 (1967).
- [45] J. M. Carlson and J. S. Langer, Mechanical model of an earthquake fault, *Phys. Rev. A* **40**, 6470 (1989).
- [46] J. D. Eshelby, The determination of the elastic field of an ellipsoidal inclusion, and related problems, *Proc. R. Soc. London Ser. A* **241**, 376 (1957).
- [47] A. Noda, T. Saito, and E. Fukuyama, Slip-deficit rate distribution along the Nankai trough, southwest Japan, with elastic lithosphere and viscoelastic asthenosphere, *J. Geophys. Res.: Sol. Ea.* **123**, 8125 (2018).
- [48] H. Gao, D. A. Schmidt, and R. J. Weldon, Scaling relationships of source parameters for slow slip events, *Bull. Seismol. Soc. Am.* **102**, 352 (2012).
- [49] R. Takagi, N. Uchida, and K. Obara, Along-strike variation and migration of long-term slow slip events in the western Nankai subduction zone, Japan, *J. Geophys. Res.: Sol. Ea.* **124**, 3853 (2019).
- [50] J. R. Sweet, K. C. Creager, and H. Houston, A family of repeating low-frequency earthquakes at the downdip edge of tremor and slip, *Geochem. Geophys. Geosyst.* **15**, 3713 (2014).
- [51] E. A. Jagla, Realistic spatial and temporal earthquake distributions in a modified Olami-Feder-Christensen model, *Phys. Rev. E* **81**, 046117 (2010).
- [52] I. Karafyllidis and A. Thanailakis, A model for predicting forest fire spreading using cellular automata, *Ecol. Model.* **99**, 87 (1997).
- [53] S. Pradhan and P. C. Hemmer, Relaxation dynamics in strained fiber bundles, *Phys. Rev. E* **75**, 056112 (2007).
- [54] D. Hamon, M. Nicodemi, and H. J. Jensen, Continuously driven OFC: A simple model of solar flare statistics, *Astron. Astrophys.* **387**, 326 (2002).
- [55] S. T. R. Pinho and C. P. C. Prado, Sequential updates for non-Abelian SOC models, *Eur. Phys. J. B* **18**, 479 (2000).
- [56] K. Ohta and S. Ide, Resolving the detailed spatiotemporal slip evolution of deep tremor in western Japan, *J. Geophys. Res.: Sol. Ea.* **122**, 10,009 (2017).
- [57] J. R. Rice, Spatio-temporal complexity of slip on a fault, *J. Geophys. Res.: Sol. Ea.* **98**, 9885 (1993).
- [58] Y. Ben-Zion and J. R. Rice, Earthquake failure sequences along a cellular fault zone in a three-dimensional elastic solid containing asperity and nonasperity regions, *J. Geophys. Res.: Sol. Ea.* **98**, 14109 (1993).
- [59] Y. Ben-Zion and J. R. Rice, Slip patterns and earthquake populations along different classes of faults in elastic solids, *J. Geophys. Res.: Sol. Ea.* **100**, 12959 (1995).
- [60] F. Wissel and B. Drossel, Transient and stationary behavior of the Olami-Feder-Christensen model, *Phys. Rev. E* **74**, 066109 (2006).
- [61] D. Weatherley, Recurrence interval statistics of cellular automaton seismicity models, *Pure Appl. Geophys.* **163**, 1933 (2006).
- [62] K. Nishida, Ambient seismic wave field, *Proc. Jpn. Acad. B* **93**, 423 (2017).